

# A Two-Branch Neural Network for Gait Recognition

Likai Wang<sup>1\*</sup> and Jinyan Chen<sup>1</sup>

<sup>1</sup>College of Intelligence and Computing, Tianjin University,  
Tianjin, 300354, China.

\*Corresponding author(s). E-mail(s): [kkww@tju.edu.cn](mailto:kkww@tju.edu.cn);  
Contributing authors: [chenjinyan@tju.edu.cn](mailto:chenjinyan@tju.edu.cn);

## Abstract

Gait recognition, a promising long-distance biometric technology, has aroused intense interest in computer vision. Existing works on gait recognition can be divided into appearance-based methods and model-based methods, which extract features from silhouettes and skeleton data, respectively. However, since appearance-based methods are greatly affected by clothing changing and carrying condition, and model-based methods are limited by the accuracy of pose estimation approaches, gait recognition remains challenging in practical applications. In order to integrate the merits of such two approaches, a two-branch neural network (NN)-based model is proposed in this paper. The method contains two branches, namely a CNN-based branch taking silhouettes as input and a GCN-based branch taking skeletons as input. In addition, two modifications are introduced into the GCN-based branch to boost the performance. First, we present a simple fully connected graph convolution operator to integrate multi-scale graph convolutions and relieve dependence on natural connections. Second, we deploy an attention module named STC-Att after each GCN block to learn spatial, temporal and channel-wise attention simultaneously. We evaluated the proposed two-branch neural network on the CASIA-B dataset. The experimental results show that our method achieves state-of-the-art performance in various conditions.

**Keywords:** gait recognition, two-branch neural network, graph convolution, convolutional neural network

# 1 Introduction

Gait recognition is a research topic for systematic study on human motion, attracting increasing interest in recent years. Due to the fact that gait can be recognized at a long-distance without the cooperation of interest-subjects while other biometric characteristics cannot, gait recognition has considerable prospect for video surveillance, crime investigation and social security. In order to extract the robust and invariant features from videos of human walking, numerous technologies have been investigated over last decades. However, the violent changes caused by exterior variations such as carrying, clothing and view changing, bring significant challenges to gait recognition.

Based on the difference of raw data, current research efforts on gait recognition can be classified into two categories, i.e., appearance-based methods and model-based methods. The first type extracts compact representations from gait silhouettes, which either compresses all gait silhouettes into one gait energy image (GEI) [1–3] or regards gait as silhouette sequences [4, 5]. However, such methods that relies on the human body shape are extremely sensitive to carrying, clothing and view changing since variations like that can alter the human appearance drastically. In contrast to the above, the second category takes raw skeleton data obtained by pose estimation algorithms as input and performs feature extraction through Convolutional Neural Networks (CNN) [6–8] or Graph Convolutional Networks (GCN) [9, 10]. Although this kind of methods can overcome the interference caused by occlusion and view-changing to a certain extent, the accuracy of pose estimation methods and the lack of information contained in skeleton data bring limitations to the improvement of gait recognition accuracy.

More specifically, GCN-based approaches [9, 10] learn the human joint movement patterns from a skeleton spatial-temporal graph with joints as nodes and bones as edges. For robust gait recognition, it is indisputable that the feature extractor should not only aggregate the information of directly connected joints, but also extract multi-scale structural features and long-range dependencies on account of strong correlations between joints that are physically apart. To implement this, existing methods deploy multi-scale graph convolutions with multiple adjacency matrix to expand the receptive field (Figure 1(a)), where every pair of nodes connected in the same adjacency matrix have the same shortest walks between them. But in practice, it is important to directly capture joint dependency between two nodes that are far apart, such as right wrist and left ankle, the movement direction and patterns of which are closely related when people walking. To achieve this, existing methods [11] apply excessive adjacency matrixes for different joint pair connections, which causes high training costs. This means that the method suffers from the balance problem between training difficulty and the effective fusion of important information from distant joints, i.e., the *distant-joint connection problem*.

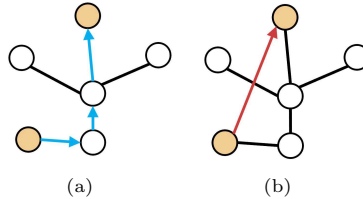


**Fig. 1** (a)Prior methods deploy multi-scale graph convolutions to aggregate information of nonadjacent vertices. (b)We propose to capture correlations between any two vertices based on full connected skeleton graph.

Motivated by the above analysis, we propose a novel two-branch neural network for gait recognition task to realize the reciprocity of appearance-based methods and model-based methods, which can significantly promote the enhancement of recognition accuracy. The appearance-based branch leverages stacked CNN to extract discriminative representations from a sequence of gait silhouettes. Besides, the model-based branch deploys multi streams, namely Joint-stream, Bone-stream and Motion-stream, to learn multi-order robust and compact representations from human skeleton data with GCN blocks. In the GCN branch, we further design two modifications for modeling the skeleton feature for gait recognition. First, to address the distant-joint connection problem as discussed above, we present a fully-connected graph structure without the natural connections between human joints, to adaptively integrate the multi-scale graph convolutions instead of the redundant adjacency matrixes for the distant joints. Second, an attention module named STC-Att is introduced to dynamically adjust the weight of convolution kernel on the spatial, the temporal and the channel dimensions. Extensive experiments indicate that the proposed model outperforms all state-of-the-art methods on the popular CASIA-B dataset. The main contributions of the proposed method are summarized as follows:

1. We propose a novel two-branch framework for gait recognition task, which combines appearance-based features and model-based features to obtain their complementary advantages. To the best of our knowledge, this is the first work to integrate the appearance- and model-based features for gait recognition.
2. In the model-based branch, we propose a simple but effective fully connected graph convolution operator that constructs a fully connected skeleton graph, which can adaptively capture the dependencies between all nodes without multi-scale convolutions. For more discriminative representations from raw skeleton data, we propose a fine-grained attention module named STC-Att to learn the spatial, temporal and channel-wise attention meanwhile.
3. Experimental results on CASIA-B dataset demonstrate that the proposed method achieves superior gait recognition performance and outperforms prior state-of-the-art methods.

## 2 Related Work

In the previous literature, there are two main ways to represent human body for gait recognition, i.e., silhouettes and skeletons. According to that gait recognition approaches can be laid in appearance-based and model-based categories.

First, gait silhouettes that can be easily computed by background subtraction and binarization are adopted most frequently in current works, which have been proven to express gait pattern with low computational expense effectively. Taking silhouettes as input, appearance-based methods usually apply two types, template or sequence to deal with temporal information. The former aggregates gait information into a single gait template, such as gait energy image (GEI) [12], chrono-gait Image (CGI) [13] and frame-difference energy images (FDEI) [14], and then extracts discriminative features from it with machine learning techniques, including linear discriminant analysis (LDA) [15], canonical correlation analysis (CCA) [16] and deep learning [2, 3, 17, 18]. In contrast, the latter directly considers gait as a sequence of silhouettes. [19] proposed a novel Auto-Encoder framework to explicitly disentangle appearance and gait feature representation from raw RGB frames, and utilize a multi-layer LSTM that can integrate pose features over time to generate gait representation for each video sequence. Some works [4, 20] created 3D tensors from spatio-temporal information available in sequences and trained with 3D CNNs. [5] learned identity information from the set and aggregated convolutional maps over the whole sequence. However, although a sequence of silhouettes contains useful gait features such as speed, gait cycle time, step length and stride length [21, 22], they are extremely sensitive to changes in the appearance of human body shape, especially due to different clothing and carrying conditions.

Second, model-based methods commonly take skeletons as raw input data, which can be captured with depth-sensing cameras [23] or be estimated from videos with pose estimation methods [24]. Since the skeleton data only contain the 2D or 3D coordinates of the human key joints, which is highly abstract information free of external noises, skeleton-based methods are more robust against viewpoint and appearance changes. [25] extract heatmaps using a CNN based pose estimate method to describe the gait information in a single frame and then adopt the LSTM to model gait sequence. [7] proposed a pose-based temporal-spatial network (PTSN) to extract the temporal features and spatial features from preprocessed gait pose using LSTM and CNN. [8] exploited human 3D pose to obtain spatio-temporal features with CNN. In addition, as recently Graph Convolutional Networks (GCN) performs well on various tasks including image classification [26], semi-supervised learning [27], and action recognition [28], some researchers attempt to leverage GCN to extract effective information from skeletons. For instance, [10] firstly applied a GCN to recognize gait and obtained remarkable performance in spite of the low dimensional feature. [9] extracted the gait information from human 2D joints based on ResGCN architecture [29]. Nevertheless, these approaches are generally more

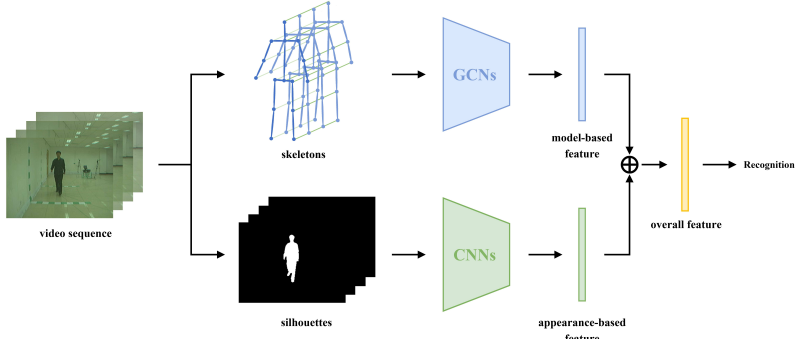


**Fig. 2** The framework of the proposed two-branch neural network.

sensitive to occlusions, due to the over-reliance on accurate detection of body joints [22].

### 3 Proposed Method

We propose a novel two-branch neural network for gait recognition in this section, which combines appearance-based approach and model-based approach to realize complementary advantages. The overall pipeline is illustrated in Figure 2. Taking raw skeletons and silhouettes respectively as input, the GCN-based branch (Section 3.1, 3.2, 3.3) and the CNN-based branch (Section 3.4) extract multi-order discriminative features. The features of all output are aggregated to obtain final compact gait signatures. We will introduce the components in detail in the following parts.

#### 3.1 Preliminaries

##### 3.1.1 Graph construction

Generally, the raw skeleton data is a sequence of vectors, each of which denotes the 2D or 3D coordinates of human key joints in one frame. According to previous works [9, 10], we need to construct a spatio-temporal graph to input to GCN, formulated as  $G = (V, E)$ . In particular, the nodes of the graph represent all joints and the edges of the graph represent the natural connections along the spatial and temporal dimension, i.e.,  $V = \{v_{ti} \mid t = 1, 2, \dots, T; i = 1, 2, \dots, N\}$ , where  $T$  represents the number of frames and  $N$  represents the number of joints. In spatial dimension, two joints with physical dependency at each frame are connected, that is, intra-frame edges  $E_s = \{(v_{ti}, v_{tj}) \mid t = 1, 2, \dots, T; i, j = 1, 2, \dots, N; i \neq j\}$ . In temporal dimension, two same joints between continuous frames are connected, that is, inter-frame edges  $E_t = \{(v_{ti}, v_{(t+1)i}) \mid t = 1, 2, \dots, T-1; i = 1, 2, \dots, N\}$ .

### 3.1.2 Spatial convolution

Spatial convolution acts on joints in the same frame, bringing in weighted average features of neighbors for each joint. The graph convolution [28] can be summarized as:

$$f_{out} = \sigma \left( \sum_k \Lambda_k^{-\frac{1}{2}} (A_k + M) \Lambda_k^{-\frac{1}{2}} f_{in} W_k \right) \quad \Lambda_k^{ii} = \sum_j A_k^{ij} \quad (1)$$

where the feature map  $f_{in}$  and  $f_{out}$  are actually tensors in  $(C, V, T)$  dimensions. Note that  $C, V, T$  denotes the number of channels, joints and frames, respectively. Besides,  $A_k$  denotes the adjacency matrix representing intra-frame connections,  $M$  is a learnable weight matrix to give minor edge corrections,  $W_j$  is the weight matrix and  $\sigma(\cdot)$  is an activation function.

### 3.1.3 Temporal convolution

The convolution on the temporal dimension is relatively simple. Similar to the classical convolution operation, we directly perform a standard 2D convolution with a fixed kernel size  $1 \times K$  on the output feature map calculated above, where  $K$  is the the number of neighbors for each node considered within the kernel receptive field. Notably, following the work in [30], for larger temporal receptive fields without increasing the kernel size, we introduce a bottleneck architecture with a fixed kernel size and different dilation rates to enhance temporal convolutional layers. Also, residual mode is applied here to boost performance.

### 3.1.4 Spatial-temporal modeling

Besides adopting factorized formulation to learn spatial-wise and temporal-wise features alternately, we also deploy a unified spatial-temporal graph convolutional operator [30], which allows that signals can be propagated directly across spacetime, to capture complex spatial-temporal joint relationships. Concretely, unfold the original graph into a spatial-temporal subgraph  $G_\tau = (V_\tau, E_\tau)$  with a sliding temporal window of size  $\tau$  and a dilation rate  $d$ , where  $V_\tau = V_1 \cup V_2 \cup \dots \cup V_\tau$  denotes all nodes of  $\tau$  frames in the sliding window and  $E_\tau$  is defined by the adjacency matrix  $A_k^{\tau, d}$  that can be computed by tiling  $A_k$  into

$$A_k^{\tau, d} = \begin{bmatrix} A_k & \dots & A_k \\ \vdots & \ddots & \vdots \\ A_k & \dots & A_k \end{bmatrix} \in \{0, 1\}^{\tau N \times \tau N} \quad (2)$$

Then, the implementation of the unified spatial-temporal convolution is derived as

$$f_{out}^{\tau, d} = \sigma \left( \sum_k \left( \Lambda_k^{\tau, d} \right)^{-\frac{1}{2}} \left( A_k^{\tau, d} + M \right) \left( \Lambda_k^{\tau, d} \right)^{-\frac{1}{2}} f_{in}^{\tau, d} W_k \right) \quad (3)$$

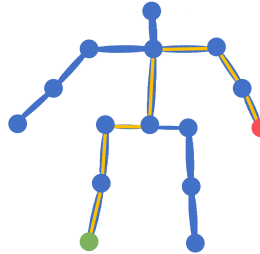


**Fig. 3** The demonstration of the raw joints data. The red vertex denotes joint right wrist, the green vertex denotes joint left ankle, and the yellow lines denote that the smallest hop between right wrist and left ankle is seven.

### 3.2 Fully Connected Graph Convolution

Under the spatial modeling in Equation 1, in order to learn long-range dependencies, current methods [30] employ multi-scale graph convolution with multiple adjacency matrixes to aggregate information of distant neighbors. Concretely,  $k$ -adjacency matrix of the graph that defines the connections between the current joint and its  $k$ -hop neighbors is first adopted to learn the dependencies at different scales, then all features are summed followed by an activation function and sent into the temporal convolution operator. The  $k$ -adjacency matrix can be formulated as

$$A_k^{i,j} = \begin{cases} 1, & i = j \\ 1, & d(v_i, v_j) = k \\ 0, & \text{otherwise} \end{cases} \quad (4)$$

However, take right wrist (the red vertex in Figure 3) for example, if all the other joints are taken into account, eight adjacency matrixes are needed since the smallest hop between the right wrist and the farthest node left ankle (the green vertex in Figure 3) is seven. On account of the inclusion of self-loops in all adjacency matrixes, the information from the right wrist joint itself will be aggregated eight times throughout the convolutional process, which leads to a bias towards the local body joint and the attenuation of other joint dependencies.

To attack the problem above, we argue that such factorized modeling is dispensable and the weight of each joint can be learned at a time. With that in mind, we propose a simple but effective fully connected graph convolution operator to integrate multi-scale convolutions and balance the contributions from the joint itself and other joints. The operator no longer relies on the physical connections and defines the adjacency matrix  $A$  as

$$A^{ij} = 1 \quad i, j = 1, 2, \dots, N \quad (5)$$

that is, each pair of nodes of the skeleton graph is interconnected. Substituting  $A_k$  with  $A$  in Equation 1, we can arrive at:

$$f_{out} = \sigma \left( \Lambda^{-\frac{1}{2}} (A + M) \Lambda^{-\frac{1}{2}} f_{in} W \right) \quad \Lambda^{ii} = \sum_j A^{ij} \quad (6)$$

Compared with multi-scale graph convolution where neighbors are divided into multiple scales based on the number of hops, the proposed fully connected convolution operator treats all nodes equally and automatically capture relationships between them. Experiments in Section 4.2 has proved that the proposed operator can enhance the recognition performance to a certain degree, particularly when taking features away from bone-wise and motion-wise data.

### 3.3 Attention Mechanism

Based on the successful application of the attention mechanism in certain fields, e.g. sequence learning [31], image captioning [32] and action recognition [33], we introduce an attention module in this section. The preliminary version of this paper [11] presented a SE block which only works on the channel dimension. However, intuitively, in addition to the focus on the channel dimension, the distinguishment of information in spatial and temporal dimension is equally critical. Actually, not all frames and joints make the same contribution to the gait recognition task, in other words, the most discriminative information generally is contained in certain joints from certain frames. Thus, to distinguish the importance of gait features on the spatial, temporal and channel dimensions, according to the works in [33], we propose a Spatial Temporal Channel Attention (STC-Att) module to dynamically adjust the weight of convolution kernel.

The concrete structure of the STC-Att module is depicted in Figure 4. Channel-wise attention (the right branch in Figure 4) [34] is performed according to the correlation between channels, which can selectively enhance useful features and suppress secondary features. Given a feature map  $F \in \mathbb{R}^{C \times V \times T}$ , the weight of each channel is learned in three steps. First, the squeeze step, where global average pooling is performed to compact gait features along the spatial and temporal dimension to a single unit, that is, the feature map is converted into  $F' \in \mathbb{R}^{C \times 1}$ . Then, the excitation step generates the weight for gait features  $W \in \mathbb{R}^{C \times 1}$  using two fully connected layers and activation functions to learn the nonlinear interaction between channels. Finally, the scale layer is adopted to complete the recalibration of gait features through channel-wise product in the reweight step.

Spatial-wise and temporal-wise attention (the left branch in Figure 4) are performed together to adaptively distinguish key joints and key frames from the whole skeleton sequence. Given a feature map  $F \in \mathbb{R}^{C \times V \times T}$ , we firstly average the spatial information along the spatial dimension into the feature map  $F_T \in \mathbb{R}^{C \times T}$  and average the temporal information along the temporal

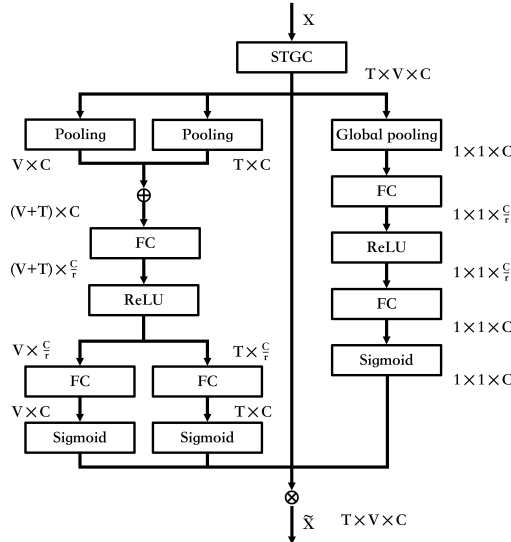


**Fig. 4** The schema of the proposed STC-Att module.

dimension into the feature map  $F_V \in \mathbb{R}^{C \times V}$ . Then, the pooled feature maps are concatenated together into feature map  $F_{VT} \in \mathbb{R}^{C \times (V+T)}$ , followed by a fully connected layer and an activation function to compress information. After that, two independent fully connected layers are deployed to learn attention scores for temporal dimension and spatial dimension respectively, which can be formulated as  $W_T \in \mathbb{R}^{C \times T}$ ,  $W_V \in \mathbb{R}^{C \times V}$ . Finally, the product of the spatial and temporal attention maps is multiplied to the input feature map for adaptive features refinement.

On the whole, by computing the importance weights for different frames, joints and channels depending on input feature maps, the proposed STC-Att module can effectively pick the information that is relatively essential to the recognition task, thereby increasing the contribution of meaningful key frames, key joints and key channels and boosting the recognition precision.

## 3.4 Model Architecture

### 3.4.1 Model-based branch

In order to abstract discriminative and robust descriptors from the raw skeleton data, spatial-temporal graph convolutional (STGC) blocks [30] are introduced as the basic component of the model, which deploys the G3D pathway that can learn complex spatial-temporal joint dependencies and the factorized pathway that captures spatial-only and temporal-only features alternately. The proposed STC-Att module is employed after each STGC block to explicitly model the channel-wise, spatial-wise and temporal-wise correlation between feature maps. Finally, a global average pooling layer and a softmax

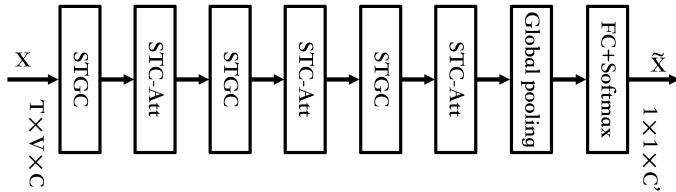


**Fig. 5** The architecture of the model-based branch.

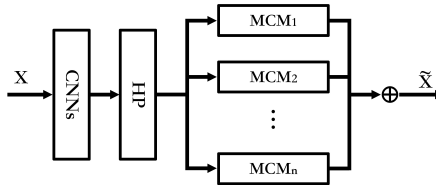


**Fig. 6** The overview of the appearance-based branch.

classifier are utilized at the end of the model for identification. The architecture of the model-based branch is depicted in Figure 5.

For further improvement of performance, we also fuse part-level features proposed in our previous work [11] in this paper to capture fine-grained information. In addition, we apply a multi-stream framework [11] that input the joint, bone and motion data to three GCN streams with the same model architecture separately and fuse all the output feature maps as the final gait representations, which has been proven to significantly boost the individual recognition.

### 3.4.2 Appearance-based branch

In the appearance-based branch, we choose a part-based model GaitPart [35] that has tremendous performance compared to other appearance-based methods to recover instructive representations from gait silhouettes. The overview of GaitPart is shown in Figure 6. As seen, the network takes a sequence of gait silhouettes as input. The frame-level part feature extractor (FPFE) composed of stacked CNNs initially generate feature maps for each frame and the horizontal pooling (HP) module horizontally splits feature maps into multi parts. Then multi parallel micro-motion capture modules (MCM) are deployed to aggregate part-level feature vectors of each corresponding human body part into a single feature vector. Finally, all the output vectors are simply concatenated as the final gait descriptors.

### 3.4.3 Two-branch network

To our knowledge, current gait recognition approaches can be classified as either appearance-based or model-based, that is, they extract gait representations either only from silhouettes or only from skeletons. However, despite its

standout recognition accuracy on normal walking, the type of methods based on silhouettes is exceedingly sensitive to changes of human body shape, which are fairly routine under the scene of different carrying and clothing conditions. On the contrary, the type of methods based on skeletons is more robust to such variations like cross-carrying and cross-clothing conditions since it does not depend on the shape of human body but only focuses on the coordinates of the key joints. Notwithstanding, these methods are limited by the correctness of pose estimation algorithms and after all, the raw skeleton data only contains the 2D coordinates of key joints which means finite information that we can mine. Consequently, model-based algorithms cannot achieve quite high accuracy for the above reasons. Inspired by that, we devise a two-branch neural network to combine the two type of methods in the hope of that they can complement one another perfectly and attain fairly high accuracy in all conditions.

Concretely, suppose that the feature vector outputted by model-based branch is  $f_m$  and the feature vector outputted by appearance-based branch is  $f_a$ , a straightforward concatenation operation is adopted to merge the two feature vectors together, which brings out the final gait descriptors for recognition. Note that because the two vectors that are obtained from completely different raw data using diverse networks have unequal size and range, a ratio  $\lambda$  is needed to adjust the rate of them. Hence, we can get the overall feature vector through  $f = f_m \oplus (\lambda \cdot f_a)$ , where  $\oplus$  means the concatenation operation. Extensive experiments in Section 4.2 demonstrates the effectiveness of the proposed fusion strategy.

## 4 Experiments

### 4.1 Dataset and Experimental Setting

#### 4.1.1 CASIA-B

To evaluate the proposed two-branch neural network, adequate experiments are conducted on the popular public gait recognition dataset CASIA-B [36], which was created by the Institute of Automation, Chinese Academy of Sciences (CASIA). For each subject, there are 11 views captured from 11 cameras at the same time, where the view angles are  $\{0^\circ, 18^\circ, 36^\circ, \dots, 180^\circ\}$ . For each view, there are 10 sequences, namely 6 sequences for normal walking (NM), 2 sequences for walking with bag (BG) and 2 sequences for walking in coat (CL). Since the dataset does not provide skeleton data, openpose [24] is exploited here to locate joints in human body from RGB videos. We choose the most representative 15 joints from the 25 estimated results as the input of model-based branch, i.e., Nose, Neck, RShoulder, RElbow, RWrist, LShoulder, LElbow, LWrist, MidHip, RHip, RKnee, RAnkle, LHip, LKnee, LAnkle. Note that all coordinates need to be normalized to the range  $[0,1]$  before entering the network. In the experiment, we follow the popular large-sample training (LT) in [5], where the first 74 subjects are grouped into training set and the rest 50

subjects belongs to the test set. In the test set, the gallery set contains the first 4 sequences of NM condition (NM01-NM04), and the probe set retains the remaining sequences (NM05-NM06, BG01-BG02, CL01-CL02). During the test, rank-1 accuracies on all gallery views are averaged where identical-view cases are excluded. For example, the accuracy of probe view  $0^\circ$  is obtained by averaging other 10 gallery views.

#### 4.1.2 Experimental setting

In model-based branch, the network is composed of 3 STGC blocks. The dimensions of feature maps outputted by each block are 96, 192, 384 in order and the strides of the latter two blocks are 2. The size of the raw skeleton data is  $2 \times 120 \times 15$ , which means that there are 120 frames for each sequence, 15 joints for each frame, and 2 channels (horizontal and vertical coordinate) for each joint. The batch size is set to 128 and the training epoch is set to 65. The initial learning rate is set to 0.1 and decays with a factor of 0.1 after the 45th and 55th epoch. In appearance-based branch, the silhouettes are aligned and resized to the size of  $64 \times 64$  as the input of CNNs. The triplet loss with the margin of 0.2 is applied to guide network training. In addition, the batch size is set to (8, 16), the maximum number of iteration is set to 8,000, the learning rate is set to 1e-4 and the momentum is set to 0.9. All experiments in this paper are performed on 1 NVIDIA 2080TI GPU.

### 4.2 Ablation Study

To validate the effectiveness of each component in the proposed method, a series of ablation studies are carried out on CASIA-B in this section.

#### 4.2.1 Effectiveness of fully connected graph convolution

We first verify the effect of the proposed fully connected graph convolution in GCN-based branch by conducting controlled experiments for three streams separately. Each set of experiments considers two scenarios, viz., the module with predefined adjacency matrix based on natural connections that represented with suffix “-P” and the module with the proposed fully connected graph convolution that represented with suffix “-F”. The results are shown in Table 1. It can be clearly seen that the model that we devise gain higher accuracies for all conditions in bone stream and motion stream, which verifies the availability of fully connected graph convolution. However, we discover that although our model improved performance under NM condition in joint stream, the accuracies for BG and CL are negatively affected to a certain extent, the possible reason for which is that unlike bone and motion data, the joint data is more dependent on the natural structure of human body. Take that into consideration, we will just apply fully connected graph convolution to bone and motion stream in the following experiments.

**Table 1** The recognition results of models with/without fully connected graph convolution.

	Accuracy(%)		
	NM	BG	CL
Multi-Stream-P	89.8	78.5	78.0
Multi-Stream-F	<b>91.3</b>	<b>79.4</b>	<b>78.5</b>
Joint-Stream-P	82.4	70.0	65.3
Joint-Stream-F	86.0	68.0	63.4
Bone-Stream-P	69.9	50.3	40.0
Bone-Stream-F	71.8	50.7	40.8
Motion-Stream-P	63.9	51.0	50.9
Motion-Stream-F	66.1	53.2	52.3

**Table 2** Ablation studies conducted on CASIA-B. The results are rank-1 accuracies averaged on all 11 views, excluding identical views.

	Accuracy(%)		
	NM	BG	CL
Multi-stream w/o Att	91.3	79.4	78.5
Multi-stream w Att	<b>91.8</b>	<b>79.8</b>	<b>79.4</b>
Joint-stream w/o Att	82.4	70.0	65.3
Joint-stream w Att	83.8	69.2	65.6
Bone-stream w/o Att	71.8	50.7	40.8
Bone-stream w Att	74.1	53.1	44.5
Motion-stream w/o Att	66.1	53.2	52.3
Motion-stream w Att	66.6	54.4	53.8

#### 4.2.2 Effectiveness of STC-Att

Here we focus on validating the proposed attention mechanism, STC-Att. In the experiments, we compare the accuracy of the model without STC-Att and the model with STC-Att embedded after GCN blocks. Notably, according to [11], channel-wise attention for joint stream is just beneficial to normal walking but harmful to other states, so we merely focus on spatial-wise and temporal-wise attention for joint stream in this paper. The results are presented in Table 2, which show the impact of attention strategy. It can be seen that after the introduction of our attention mechanism, the recognition rates of the multi-stream and each single-stream network have been improved in almost all conditions, which reveals the superiority of STC-Att to capture the discriminative gait representations.

#### 4.2.3 Discussion of two-branch fusion

As mentioned in Section 3.4, to combine model-branch and appearance-based branch, a ratio  $\lambda$  is needed to weigh the disparity between them. In order to determine the most suitable ratio for the best performance of the two-branch network, we compare different values of  $\lambda$ , namely from 300 to 500 with 50 as interval. The averaged accuracies are shown in Table 3. The first two lines show the averaged accuracies of model-branch and appearance-based branch respectively. We observe that as the value of  $\lambda$  increases, the accuracy rate

**Table 3** Averaged rank-1 accuracies with different values of  $\lambda$ .

	Accuracy(%)			
	NM	BG	CL	Mean
model-based branch	91.8	79.8	79.4	83.67
appearance-based branch	91.5	81.7	68.6	80.60
$\lambda = 300$	97.0	92.8	<b>93.4</b>	94.38
$\lambda = 350$	97.5	93.4	93.1	94.65
$\lambda = 400$	97.7	93.8	92.7	<b>94.74</b>
$\lambda = 450$	<b>97.7</b>	<b>93.9</b>	91.9	94.51
$\lambda = 500$	97.6	93.5	90.8	93.98

under all conditions shows a trend of first increasing and then decreasing. NM and BG condition get the best results with setting  $\lambda = 450$  and CL condition gets the best results with setting  $\lambda = 300$ . In addition, we calculate the mean value of accuracies under the three conditions (shown in the last column). Considering that the model should perform well in various states, we choose  $\lambda = 400$  with the highest mean value as the final ratio.

More specifically, we compare the recognition rates of the single branch and the fused branch at 4 different probe angles with  $36^\circ$  interval, namely  $36^\circ$ ,  $72^\circ$ ,  $108^\circ$  and  $144^\circ$ . The comparisons are depicted in Figure 7, where each row represents a probe angle and each column represents a walking condition. As clearly seen in Figure 7, the fused network outperforms the model-only and appearance-only network at the vast majority of pairs of probe angle and gallery angle under all walking conditions. The results demonstrate that the proposed two-branch network can achieve complementation of the two types of methods and dramatically improve performance.

### 4.3 Comparisons with State-of-art Methods

In this section, we compare the proposed two-branch neural network to additional state-of-the-art gait recognition methods with the same experimental settings systematically and comprehensively, including GaitGraph [9], MS-Gait [11], GaitSet [5] and GaitPart [35]. Among that, the first two methods belong to model-based and the last two methods belong to appearance-based. Notably, the accuracies of the compared approaches are directly cited from their original papers. The detailed results are listed in Table 4. From the view of results, the proposed model exceeds all existing approaches and presents the best performance under various walking conditions on CASIA-B. Especially in the CL condition, the accuracy of ours increases by 14% compared with GaitPart [35], which can indicate that the proposed network have great utility in handling with the presence of occlusion and abstracting discriminative and fine-grained gait descriptors. Apart from that, it is worth mentioning that our work is the first to devise a two-branch network to merge gait features learned from silhouettes and from skeletons, and the results has proven the effectiveness of this combination.



Fig. 7 Comparison of the single branch and the fused branch at different probe angles.

## 5 Conclusion

In this paper, we presented a novel two-branch neural network composed of a CNN-based branch extracting gait features from silhouettes and a GCN-based branch extracting gait features from skeletons. We also provide a concise but

**Table 4** Comparison of gait recognition performance on CASIA-B.

Gallery angle NM01-NM04		0° – 180°											
Probe angle		0°	18°	36°	54°	72°	90°	108°	126°	144°	162°	180°	Mean
NM	GaitGraph[9]	85.3	88.5	91.0	92.5	87.2	86.5	88.4	89.2	87.9	85.9	81.9	87.7
	MS-Gait[11]	89.4	91.7	91.6	90.2	90.6	90.6	90.4	90.9	90.4	88.5	85.6	90.0
	GaitSet[5]	90.8	97.9	<b>99.4</b>	96.9	93.6	91.7	95.0	97.8	98.9	96.8	85.8	95.0
	GaitPart[35]	94.1	<b>98.6</b>	99.3	<b>98.5</b>	94.0	92.3	95.9	98.4	<b>99.2</b>	97.8	90.4	96.2
	Ours	<b>97.0</b>	97.9	98.4	98.3	<b>97.2</b>	<b>97.3</b>	<b>98.2</b>	<b>98.4</b>	98.3	<b>98.1</b>	<b>96.0</b>	<b>97.7</b>
BG	GaitGraph[9]	75.8	76.7	75.9	76.1	71.4	73.9	78.0	74.7	75.4	75.4	69.2	74.8
	MS-Gait[11]	75.7	84.8	83.7	83.2	80.6	80.1	82.2	79.8	79.1	75.9	71.1	79.7
	GaitSet[5]	83.8	91.2	91.8	88.8	88.3	81.0	84.1	90.0	92.2	<b>94.4</b>	79.0	87.2
	GaitPart[35]	89.1	<b>94.8</b>	<b>96.7</b>	<b>95.1</b>	88.3	<b>94.9</b>	89.0	93.5	<b>96.1</b>	93.8	85.8	91.5
	Ours	<b>91.9</b>	94.6	96.4	94.3	<b>94.4</b>	91.6	<b>94.1</b>	<b>95.4</b>	95.5	93.9	<b>89.5</b>	<b>93.8</b>
CL	GaitGraph[9]	69.6	66.1	68.8	67.2	64.5	62.0	69.5	65.6	65.7	66.1	64.3	66.3
	MS-Gait[11]	75.1	79.7	80.5	84.7	84.0	82.4	79.8	80.4	78.3	78.0	70.9	79.4
	GaitSet[5]	61.4	75.4	80.7	77.3	72.1	70.1	71.5	73.5	73.5	68.4	50.0	70.4
	GaitPart[35]	70.7	85.5	86.9	83.3	77.1	72.5	76.9	82.2	83.8	80.2	66.5	78.7
	Ours	<b>87.4</b>	<b>96.0</b>	<b>97.0</b>	<b>94.6</b>	<b>94.0</b>	<b>90.1</b>	<b>91.5</b>	<b>94.1</b>	<b>93.8</b>	<b>92.6</b>	<b>88.5</b>	<b>92.7</b>

effective fully connected graph convolution operator and an attention module to enhance the recognition performance. Extensive experiments based on the CASIA-B database shows that our method surpasses all the appearance-based and model-based methods under all walking conditions, showing its great potential in dealing with the presence of viewpoint, carrying and clothing condition variations. However, the fusion mode of the two types of approaches employed in this paper is simply concatenation operation. We will explore better in-depth integration strategy to further improve gait recognition accuracy in the future.

## Declarations

This work was supported by Tianjin Research Innovation Project for Post-graduate Students under Grant 2021YJSB174.

## References

- [1] He, Y., Zhang, J., Shan, H., Wang, L.: Multi-task gans for view-specific feature learning in gait recognition. *IEEE Transactions on Information Forensics and Security* **14**(1), 102–113 (2018)
- [2] Takemura, N., Makihara, Y., Muramatsu, D., Echigo, T., Yagi, Y.: On input/output architectures for convolutional neural network-based cross-view gait recognition. *IEEE Transactions on Circuits and Systems for Video Technology* **29**(9), 2708–2719 (2017)
- [3] Wu, Z., Huang, Y., Wang, L., Wang, X., Tan, T.: A comprehensive study on cross-view gait based human identification with deep cnns. *IEEE transactions on pattern analysis and machine intelligence* **39**(2), 209–226 (2016)
- [4] Wolf, T., Babaee, M., Rigoll, G.: Multi-view gait recognition using 3d convolutional neural networks. In: 2016 IEEE International Conference on Image Processing (ICIP), pp. 4165–4169 (2016). IEEE

- [5] Chao, H., He, Y., Zhang, J., Feng, J.: Gaitset: Regarding gait as a set for cross-view gait recognition. In: Proceedings of the AAAI Conference on Artificial Intelligence, vol. 33, pp. 8126–8133 (2019)
- [6] An, W., Liao, R., Yu, S., Huang, Y., Yuen, P.C.: Improving gait recognition with 3d pose estimation. In: Chinese Conference on Biometric Recognition, pp. 137–147 (2018). Springer
- [7] Liao, R., Cao, C., Garcia, E.B., Yu, S., Huang, Y.: Pose-based temporal-spatial network (ptsn) for gait recognition with carrying and clothing variations. In: Chinese Conference on Biometric Recognition, pp. 474–483 (2017). Springer
- [8] Liao, R., Yu, S., An, W., Huang, Y.: A model-based gait recognition method with body pose and human prior knowledge. *Pattern Recognition* **98**, 107069 (2020)
- [9] Teepe, T., Khan, A., Gilg, J., Herzog, F., Hörmann, S., Rigoll, G.: Gait-graph: Graph convolutional network for skeleton-based gait recognition. arXiv preprint arXiv:2101.11228 (2021)
- [10] Li, N., Zhao, X., Ma, C.: Jointsgait: A model-based gait recognition method based on gait graph convolutional networks and joints relationship pyramid mapping. arXiv preprint arXiv:2005.08625 (2020)
- [11] Wang, L., Chen, J., Chen, Z., Liu, Y., Yang, H.: Multi-stream part-fused graph convolutional networks for skeleton-based gait recognition. *Connection Science*, 1–18 (2022)
- [12] Han, J., Bhanu, B.: Individual recognition using gait energy image. *IEEE transactions on pattern analysis and machine intelligence* **28**(2), 316–322 (2005)
- [13] Wang, C., Zhang, J., Pu, J., Yuan, X., Wang, L.: Chrono-gait image: A novel temporal template for gait recognition. In: European Conference on Computer Vision, pp. 257–270 (2010). Springer
- [14] Chen, C., Liang, J., Zhao, H., Hu, H., Tian, J.: Frame difference energy image for gait recognition with incomplete silhouettes. *Pattern Recognition Letters* **30**(11), 977–984 (2009)
- [15] Bashir, K., Xiang, T., Gong, S.: Gait recognition without subject cooperation. *Pattern Recognition Letters* **31**(13), 2052–2060 (2010)
- [16] Xing, X., Wang, K., Yan, T., Lv, Z.: Complete canonical correlation analysis with application to multi-view gait recognition. *Pattern Recognition* **50**, 107–117 (2016)

- [17] Yu, S., Chen, H., Wang, Q., Shen, L., Huang, Y.: Invariant feature extraction for gait recognition using only one uniform model. *Neurocomputing* **239**, 81–93 (2017)
- [18] Shiraga, K., Makihara, Y., Muramatsu, D., Echigo, T., Yagi, Y.: Geinet: View-invariant gait recognition using a convolutional neural network. In: 2016 International Conference on Biometrics (ICB), pp. 1–8 (2016). IEEE
- [19] Zhang, Z., Tran, L., Yin, X., Atoum, Y., Liu, X., Wan, J., Wang, N.: Gait recognition via disentangled representation learning. In: Proceedings of the IEEE/CVF Conference on Computer Vision and Pattern Recognition, pp. 4710–4719 (2019)
- [20] Lin, B., Zhang, S., Bao, F.: Gait recognition with multiple-temporal-scale 3d convolutional neural network. In: Proceedings of the 28th ACM International Conference on Multimedia, pp. 3054–3062 (2020)
- [21] Nieto-Hidalgo, M., Ferrández-Pastor, F.J., Valdivieso-Sarabia, R.J., Mora-Pascual, J., García-Chamizo, J.M.: Vision based extraction of dynamic gait features focused on feet movement using rgb camera. In: Ambient Intelligence for Health, pp. 155–166 (2015). Springer
- [22] Verlekar, T.: Gait analysis in unconstrained environments. PhD thesis, Ph. D. dissertation, Electrical and Computer Engineering, Instituto Superior ... (2019)
- [23] Gianaria, E., Balossino, N., Grangetto, M., Lucenteforte, M.: Gait characterization using dynamic skeleton acquisition. In: 2013 IEEE 15th International Workshop on Multimedia Signal Processing (MMSP), pp. 440–445 (2013). IEEE
- [24] Cao, Z., Hidalgo, G., Simon, T., Wei, S.-E., Sheikh, Y.: Openpose: real-time multi-person 2d pose estimation using part affinity fields. *IEEE transactions on pattern analysis and machine intelligence* **43**(1), 172–186 (2019)
- [25] Feng, Y., Li, Y., Luo, J.: Learning effective gait features using lstm. In: 2016 23rd International Conference on Pattern Recognition (ICPR), pp. 325–330 (2016). IEEE
- [26] Bruna, J., Zaremba, W., Szlam, A., LeCun, Y.: Spectral networks and locally connected networks on graphs. *arXiv preprint arXiv:1312.6203* (2013)
- [27] Kipf, T.N., Welling, M.: Semi-supervised classification with graph convolutional networks. *arXiv preprint arXiv:1609.02907* (2016)

- [28] Yan, S., Xiong, Y., Lin, D.: Spatial temporal graph convolutional networks for skeleton-based action recognition. In: Thirty-second AAAI Conference on Artificial Intelligence (2018)
- [29] Song, Y.-F., Zhang, Z., Shan, C., Wang, L.: Stronger, faster and more explainable: A graph convolutional baseline for skeleton-based action recognition. In: Proceedings of the 28th ACM International Conference on Multimedia, pp. 1625–1633 (2020)
- [30] Liu, Z., Zhang, H., Chen, Z., Wang, Z., Ouyang, W.: Disentangling and unifying graph convolutions for skeleton-based action recognition. In: Proceedings of the IEEE/CVF Conference on Computer Vision and Pattern Recognition, pp. 143–152 (2020)
- [31] Bluche, T.: Joint line segmentation and transcription for end-to-end handwritten paragraph recognition. Advances in Neural Information Processing Systems **29**, 838–846 (2016)
- [32] Chen, L., Zhang, H., Xiao, J., Nie, L., Shao, J., Liu, W., Chua, T.-S.: Sca-cnn: Spatial and channel-wise attention in convolutional networks for image captioning. In: Proceedings of the IEEE Conference on Computer Vision and Pattern Recognition, pp. 5659–5667 (2017)
- [33] Song, Y.-F., Zhang, Z., Shan, C., Wang, L.: Constructing stronger and faster baselines for skeleton-based action recognition. arXiv preprint arXiv:2106.15125 (2021)
- [34] Hu, J., Shen, L., Sun, G.: Squeeze-and-excitation networks. In: Proceedings of the IEEE Conference on Computer Vision and Pattern Recognition, pp. 7132–7141 (2018)
- [35] Fan, C., Peng, Y., Cao, C., Liu, X., Hou, S., Chi, J., Huang, Y., Li, Q., He, Z.: Gaitpart: Temporal part-based model for gait recognition. In: Proceedings of the IEEE/CVF Conference on Computer Vision and Pattern Recognition, pp. 14225–14233 (2020)
- [36] Yu, S., Tan, D., Tan, T.: A framework for evaluating the effect of view angle, clothing and carrying condition on gait recognition. In: 18th International Conference on Pattern Recognition (ICPR’06), vol. 4, pp. 441–444 (2006). IEEE